Well-seismic bandwidth and time-lapse seismic characterization related to CO_2 injection and fluid substitution: physical considerations

Yinbin Liu and Don C. Lawton

ABSTRACT

Reservoirs are commonly heterogeneous. Injection of CO_2 (or other fluids) related to enhanced oil recovery (EOR) operations may cause strong lateral and depth-dependent changes of heterogeneity both within the reservoir and in the surrounding formations. A seismic signal propagating through the reservoir and the surrounding formations before and after the injection undergoes different velocity dispersion and amplitude attenuation, which result in time shifts and waveform distortion. This paper discusses the physical aspects of well log integration with seismic and time-lapse seismic characterization based on a thinly layered model (1D heterogeneity). The results show that discrete layering and interval multiple reflections (or scattering) within sedimentary sequences have a significant influence on synthetic seismograms. The velocity and density perturbations inside and outside the reservoir will mainly result in the time-lapse amplitude anomaly at the top of the reservoir and the local coda wave distortion from near the top of the reservoir to the strong basal reflection below the reservoir (BBR). The distortion of the coda wave is highly dependent on the magnitudes of medium perturbations. Large perturbations may cause time sag for the basal reflection as well as later events, which mainly include primary reflections. Those results have important implications for time-lapse seismic monitoring.

INTRODUCTION

Sonic logs and seismic surveys measure the acoustic responses of the earth with different resolutions. Sonic logs can usually identify individual sedimentary layers at tens of centimetres in thickness (borehole scale), and a seismic reflector is usually the overall response of many sedimentary layers at a scale of tens of meters. Physically speaking, seismic and sonic logs should be thoroughly integrated. There is a need to physically fill the gap between sonic bandwidth and seismic bandwidth so as to identify small-scale reservoir and to monitor reservoir characterization from seismic data.

Production of hydrocarbons and injection of CO_2 (or other fluids) related to EOR operations will cause changes in sonic velocity and density both inside the reservoir (changes of both fluid properties and stress) and outside the reservoir (change of stress). These changes may be observed on time-lapse seismic data. For example, we can observe the waveform distortion in the reservoir section and “pushdown” effect or time sag for reflections below the reservoir (e.g., Arts et al., 2004; Calvert, 2005). However, the corresponding relationships between the changes of time-lapse seismic data and fluid saturation and distribution have not been established. The multiple scattering of seismic wave within heterogeneous reservoirs remains poorly understood.

Seismic wave propagation and scattering in strong 1D heterogeneity can be modeled by a propagator matrix approach (e.g., Liu and Schmitt, 2006). In this paper we first study frequency-dependent seismic reflections for a blocked wedge model. Then the influence of interval multiple scattering on seismic reflection is analyzed. Acoustic velocity associated with rock deformation processes is discussed. Finally, time-lapse seismic characterization is studied by blocking the reservoir and the surrounding formations into many thin layers with depth-dependent velocity and density perturbations.

WELL-SEISMIC BANDWIDTH

Primary and multiples

Figure 1a shows sonic and density logs from a well in central Alberta. The changes of density and velocity are large in the overburden and are slightly larger in the reservoir section than those in its surrounding formations. In this study we block the logs from 308 m to 2221 m into about 1350 layers. Figures 1b and 1c show the blocked density and velocity logs and the corresponding perturbations inside and outside the reservoir caused by CO_2 injection. Figure 2 shows the normal reflection synthetic seismograms for a 50 Hz zero-phase Ricker wavelet source before medium perturbations. The blue and red lines stand for the results from primary reflections (conventional convolution model) and multiple reflections (propagator matrix, which includes both primary and multiples), respectively. It can be seen that there is a large difference between synthetic seismograms when multiples are included. The longer the propagation time or distance, the larger the waveform distortion is. The amplitude difference at about 1300 ms is up to about 500%. This is because multiple scattering will redistribute seismic energy, a long propagation time or traveling distance will include more multiple waves. The multiple scattering in a strong 1D heterogeneity results in large waveform distortion (amplitude, frequency, and phase or time).

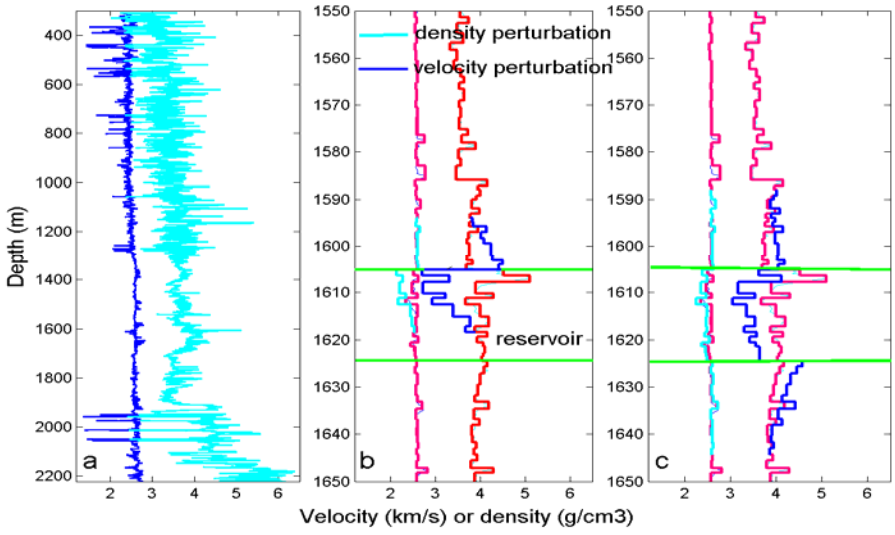

FIG. 1. Density and sonic logs and density and velocity perturbations inside and outside the reservoir.

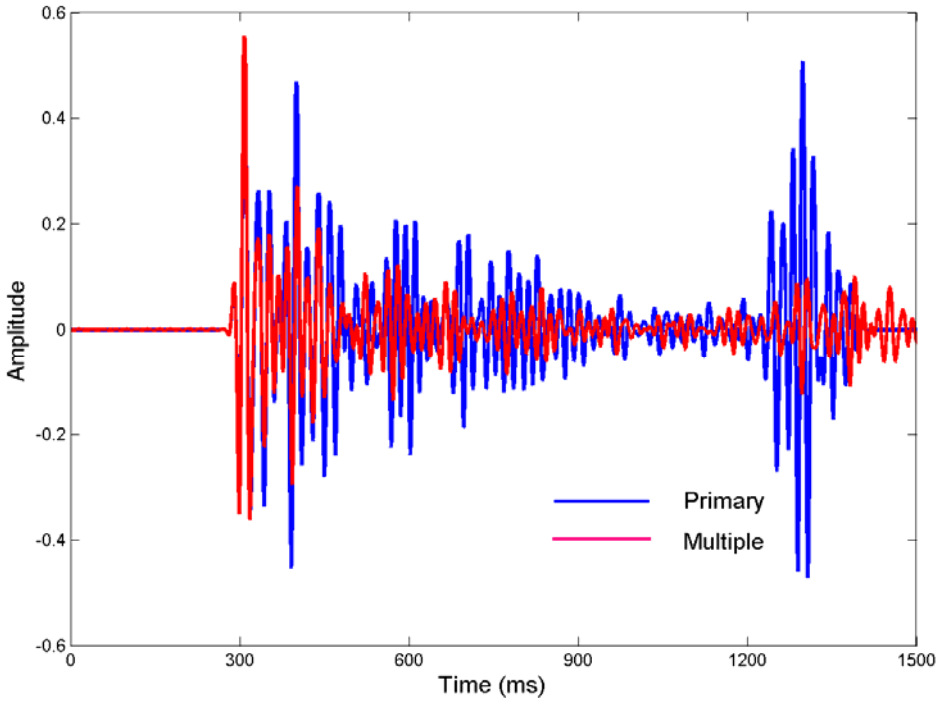

FIG. 2. Primary (blue) and multiple (red) synthetic seismograms before medium perturbations.

Frequency-dependent seismic reflections

Understanding for scale-dependent velocity dispersion and amplitude attenuation of seismic waves (well-seismic bandwidth) within sedimentary sequences is a key issue for subtle reservoir characterizations. Figure 3 (brown line) is an upward-coarsening wedge model (Hilterman, 2001) with velocity changes from 2250 m/s to 4500 m/s and density changes from 2.393 g/cm^3 to 2.8716 g/cm^3 over a 200 m depth. The model can be approximately blocked into 20 transitional layers, each 10 m thick (the velocity increases in a step of 112.5 m/s and the density increases in a step of 0.02393 g/cm^3). A propagator matrix method is employed to study the reflection characterization. Figure 3 (blue lines) shows the calculated normal seismic reflections for a zero-phase Ricker wavelet source with dominant frequencies from 20 Hz to 400 Hz. The corresponding λ/d changes are from 8.5 to 0.4. The time triggers are the starting points of the first arrivals (green line). The waveforms show polarity reversals because the reflections are from high to low impedance layers. It can be seen that seismic reflections are the cumulative effects of the transitional layers, and main waveform distortion is from a strong and abrupt contrast of acoustic impedance, which is on the top boundary. The interference of interbed multiples causes coda waves, which follow the main reflection, its frequency increases and amplitude decreases with propagation time for $\lambda/d >$ about 1 (scattering region). It is difficult to identify the reflections for the individual transitional layers for low frequency incident waves ($\lambda/d >$ about 2). However, the coda waves produced by multiple reflections or scattering for high frequency incident waves (about 2 $> \lambda/d >$ about 0.8) can be clearly seen. As λ/d decreases further ($\lambda/d <$ about 0.8), the later arriving reflections can be identified by ray medium theory.

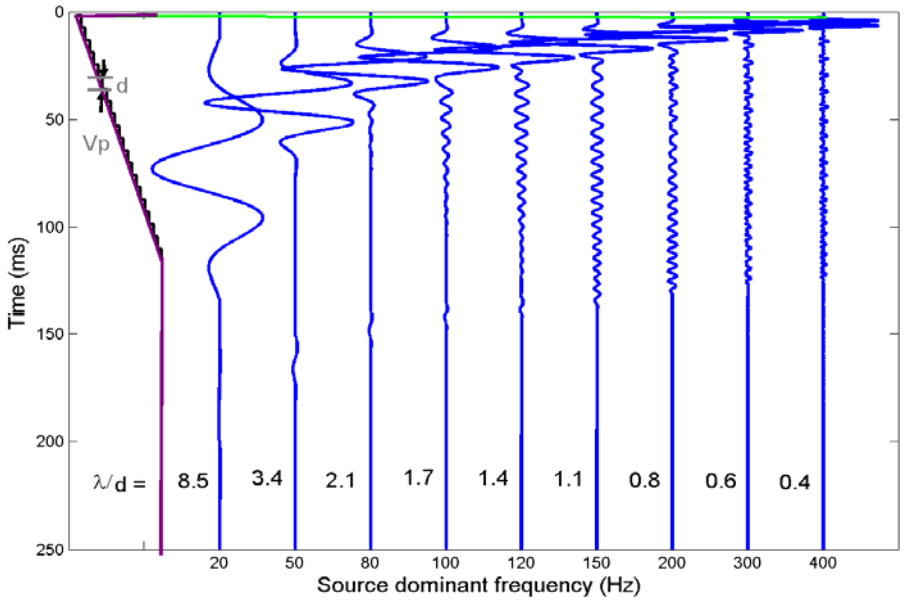

FIG. 3. Reflection synthetics of a blocked upward-coarsening wedge model for different frequency Ricker wavelet sources.

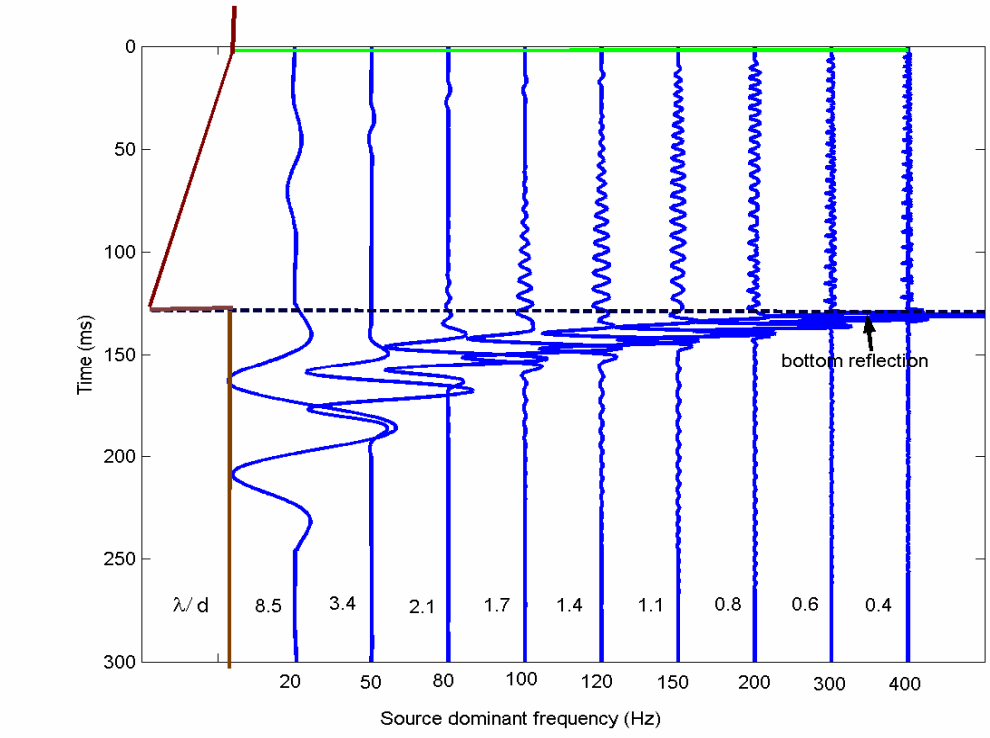

FIG. 4. Reflection synthetics of a blocked downward-coarsening wedge model for different frequency Ricker wavelet sources.

Figure 4 shows the calculated normal reflections for a blocked wedge model with velocity changes from 4500 m/s to 2250 m/s and density changes from 2.8716 g/cm^3 to 2.393 g/cm^3 over a 200 m depth (the other parameters are the same as Figure 3). The waveforms in Figure 4 show the opposite features of Figure 3. The main waveform distortion is from a strong impedance contrast, which is on the bottom boundary and has the same polarity as the source because the reflections are from low to high impedance media. The coda waves precede the main reflection, the frequency decreases and amplitude increases with propagation time for $\lambda/d >$ about 1. This indicates the frequency characterization of coda waves is related to small-scale heterogeneity of the medium. For high frequency incident waves, the multiple reflections can be identified based on ray theory.

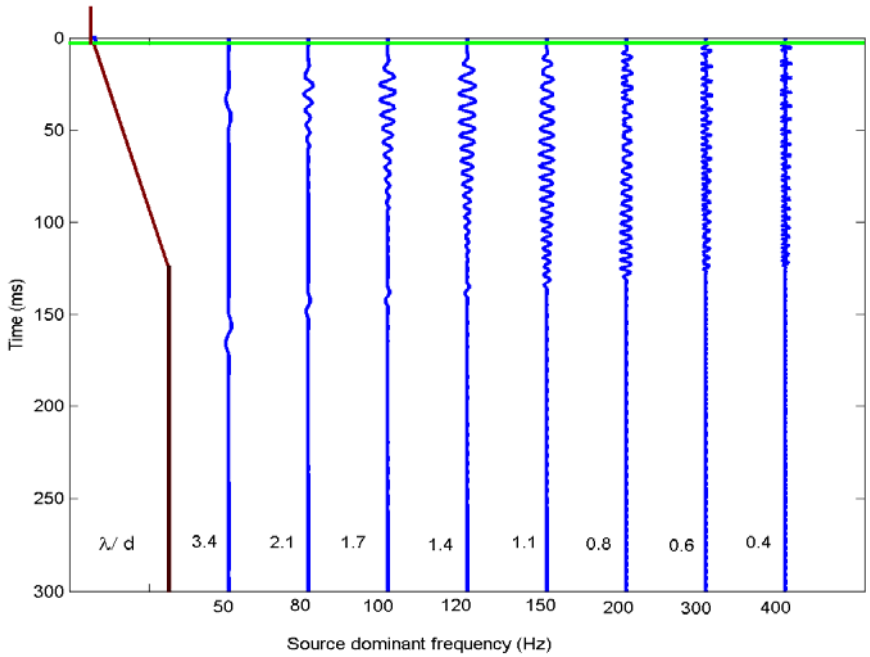

FIG. 5. Reflection synthetics of a blocked transitional model for different frequency Ricker wavelet sources.

Figure 5 shows the calculated normal reflections for a blocked transitional layer with velocity changes from 2250 m/s to 4500 m/s and density changes from 2.393 g/cm^3 to 2.8716 g/cm^3 over a 200 m depth (the other parameters are the same as Figure 3). It can be seen no strong reflection in Figure 5 because the model is a blocked transitional layers. Multiple scattering causes frequency-dependent coda wave, its frequency increases and amplitude decreases as propagation time.

ACOUSTIC VELOCITY IN ROCK DEFORMATION PROCESSES

Biot-Gassmann's equations and rock deformation

Biot-Gassmann's equations, based on linear elasticity assumptions, commonly are used to predict seismic velocity changes resulting from CO_2 and other fluid injection (e.g., Mavko et al., 1998). However, practical time-lapse seismic data show Biot-Gassmann's equation usually underestimates the velocity changes (Jenkins et al., 1997; Li, 2003; Ng et al., 2005). During production of hydrocarbons and injection of CO_2 and other fluids, the reservoirs and the surrounding rocks undergo both elastic and inelastic deformation caused by pore fluid pressure changes. These include elasticity, dilatancy, pore collapse, and normal compaction or consolidation (Scott et al., 1998). As strain increases, the sonic velocity tends to increase in elastic regions, decrease in dilatancy and pore collapse regions, and increase in the normal consolidation regions. Mechanical rock damage will change the elastic moduli of the skeletons of porous rocks (inelasticity). Pore collapse may dramatically decrease propagation velocity and increase amplitude attenuation. For example, the sonic velocity of unconsolidated sands may be much less than that of the saturated fluid (Kvamme et al., 1997). This is because the acoustic property of an unconsolidated fluid/solid two-phase medium is dominated by the compressibility of a fluid and the density of a solid. Biot-Gassmann's equations, which assume the same elastic moduli of skeletons before and after CO_2 injection, cannot well explain the observed time-lapse seismic data.

CO_2 injection model

During injection into the reservoir in Figure 1, CO_2 tends to move up because of buoyant force and first substitutes or mixes with the original pore fluids near the top of the reservoir (or also leaks occasionally into the formations above the reservoir), and causes the changes of pore fluid saturation within reservoir and stress changes both inside reservoir (vertical elongation) and the surrounding rocks (vertical contraction, Tura et al., 2005). The changes in velocity and density will tend to decrease with depth inside the reservoir. The thickness of the reservoir sand in the studied area is about 18.5 m (depth from about 1605 m to 1623.5 m), which is blocked into 14 thin layers in Figures 1b and 1c (the thickness of each blocked layer is much less than the seismic wavelength). Total thickness of the perturbations within the reservoir is basically the same as that of the surrounding formations. In this study, we build three kinds of models to simulate depth-dependent velocity and density perturbations: (1) perturbations only inside the reservoir (Figure 1b); (2) perturbations both inside and above the reservoir (Figure 1b); (3) perturbations both inside and outside the reservoir (Figure 1c). The depth-dependent perturbations can be incorporated into a layered model by blocking the reservoir and the surrounding rocks into many thin layers (1D heterogeneity). The large change of heterogeneity near the top of the reservoir produced by CO_2 injection is simulated by the thin layers with large perturbations. The thickness changes caused by reservoir compaction or elongation and surface subsidence or rising (Sen and Settari, 2005) are ignored in this study.

TIME-LAPSE SYNTHETIC SEISMIC CHARACTERIZATION

Time-lapse seismic anomalies are the responses of velocity and density perturbations inside the reservoir and the surrounding formations (Lines et al., 2003). Figure 6 shows the influence of depth-dependent velocity and density perturbations both inside and above the reservoir on seismic reflections for a 50 Hz zero-phase Ricker wavelet. For each injected CO_2 thickness, the depth-dependent velocity and density perturbations are from -40% to 0% and from -15% to 0%, and the corresponding perturbations above the reservoir are from 20% to 0% and from 1% to 0%, respectively. Figure 1b shows that the velocity and density perturbations inside the reservoir (12.0 m) and above the reservoir (12.0 m). The three trace group to the left in Figure 6 correspond to the seismic reflections and the three trace group to the right correspond to the seismic reflection differences for different velocity and density perturbations. The red lines show a seismic reflection before medium perturbations. The blue and green lines are the seismic reflections or the differences from only the reservoir perturbations and from both inside and above the reservoir perturbations, respectively.

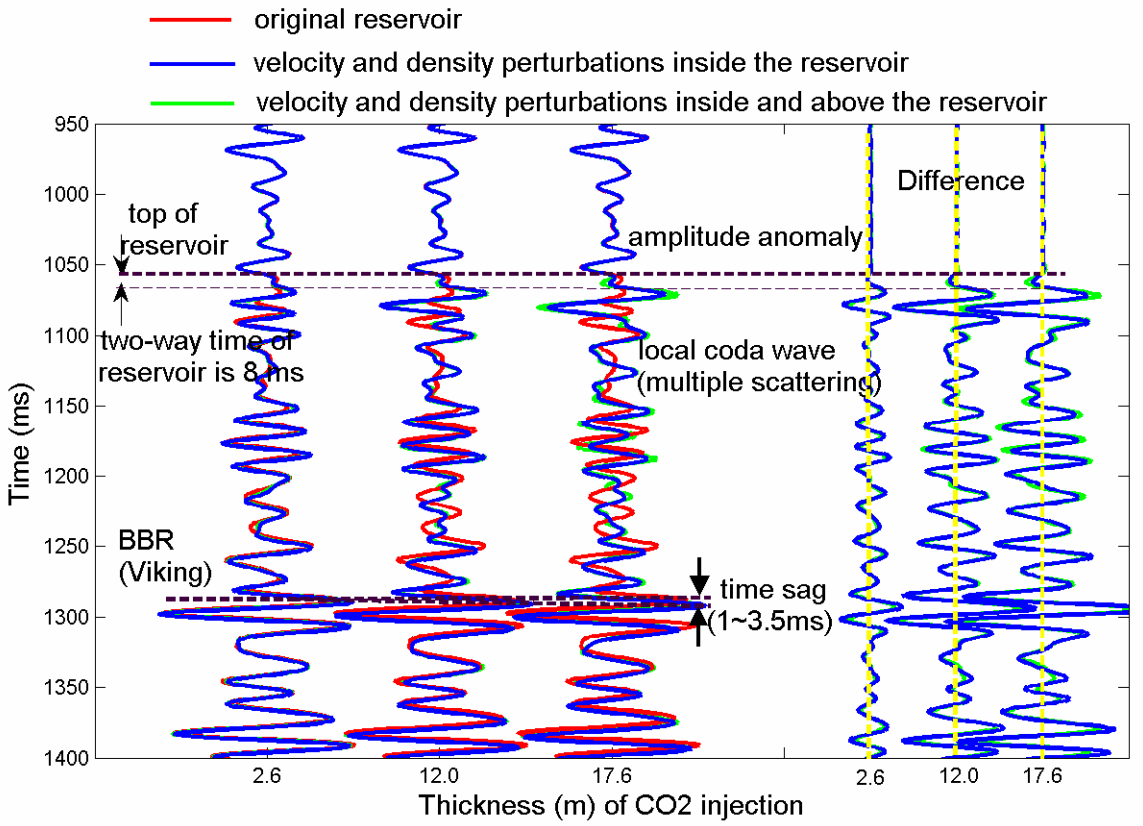

FIG. 6. Influence of velocity and density perturbations both inside and above the reservoir on seismic reflections.

Figure 7 shows the influence of velocity and density perturbations both inside and outside the reservoir on seismic reflections (entire reservoir perturbations). The velocity and density perturbations outside the reservoir are from 10% to 0% and from 1% to 0%,

respectively, and the velocity and density perturbations inside the reservoir are given in 3 values: (1) -10% velocity perturbation and -5% density perturbation for the entire reservoir (see Figure 1c); (2) the perturbation changes from the top to the bottom of the reservoir are from -30% to -10% for the velocities and -10% to -5% for the densities; (3) is the same as (2) except from -40% to -20% for the velocities. The red lines show a seismic reflection before medium perturbation and the blue lines stand for seismic reflections and the corresponding difference after different velocity and density perturbations. Figures 6 and 7 show that the top reservoir reflection is at about 1060 ms and the base reflection below the reservoir (BBR, Viking formation) is at about 1280 ms, the later is a strong seismic reflection because of strong impedance contrasts for this event.

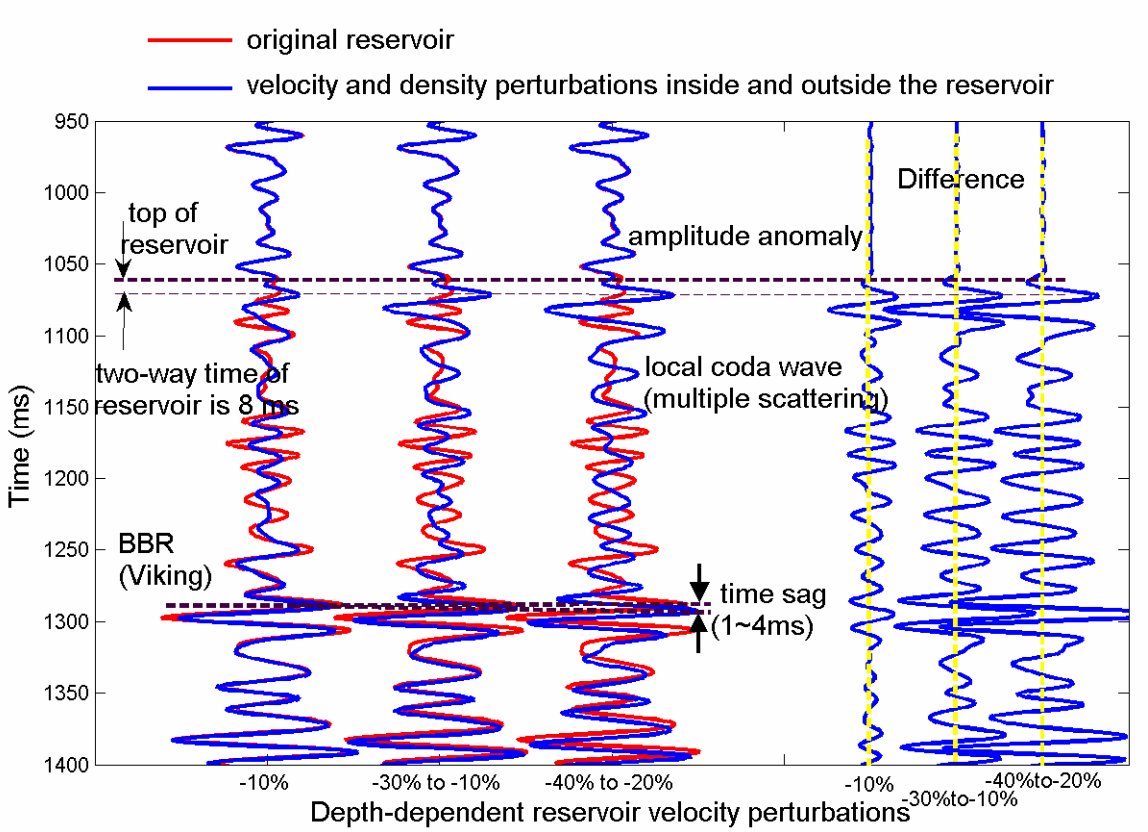

FIG. 7. Influence of velocity and density perturbations both inside and outside the reservoir on seismic reflections.

Figures 6 and 7 show the start times of waveform distortions for either different perturbation regions (perturbation either inside or inside and above or inside and outside the reservoir) or different perturbation thicknesses are almost the same. This indicates the influence of velocity and density perturbations on the arrival times of the top of the reservoir is small. However, the influences may be significant for the reflection strengths on the top of the reservoir (large amplitude change). The time-lapse amplitude anomaly may go up to 100% or more. This is because the depth-dependent velocity and density

perturbations produce the cumulative effects on the boundaries of the top and bottom of the reservoir as discussed in Figures 3 and 4.

The two-way travel time of the reservoir in Figures 6 and 7 is about 8ms. However, the waveform distortions mainly take place at the section from near the top of the reservoir to the BBR reflection, which is much longer than the two-way travel time of the reservoir. This is because the seismic reflections from both the reservoir and below the reservoir undergo multiple scattering within the reservoir, which causes different waveform distortion before and after CO_2 injection. The overall differences of time-lapse seismic reflections increase with increasing medium perturbations (amount of CO_2 injection). The multiple scattering waves caused by CO_2 injection are usually weaker than a BBR primary reflection or later events, which are strong seismic reflections because of strong impedance contrast. Therefore, the BBR reflection mainly includes primary reflections and undergoes small waveform distortion after medium perturbations. However, the BBR reflection or later events, which travel through the reservoir twice, may cause time sag or "pushdown" effect and amplitude anomaly as seen in Figures 6 and 7. The time sags from the left to the right is from about 1 ms to 3.5 ms in Figure 6 and from 1 ms to 4 ms in Figure 7.

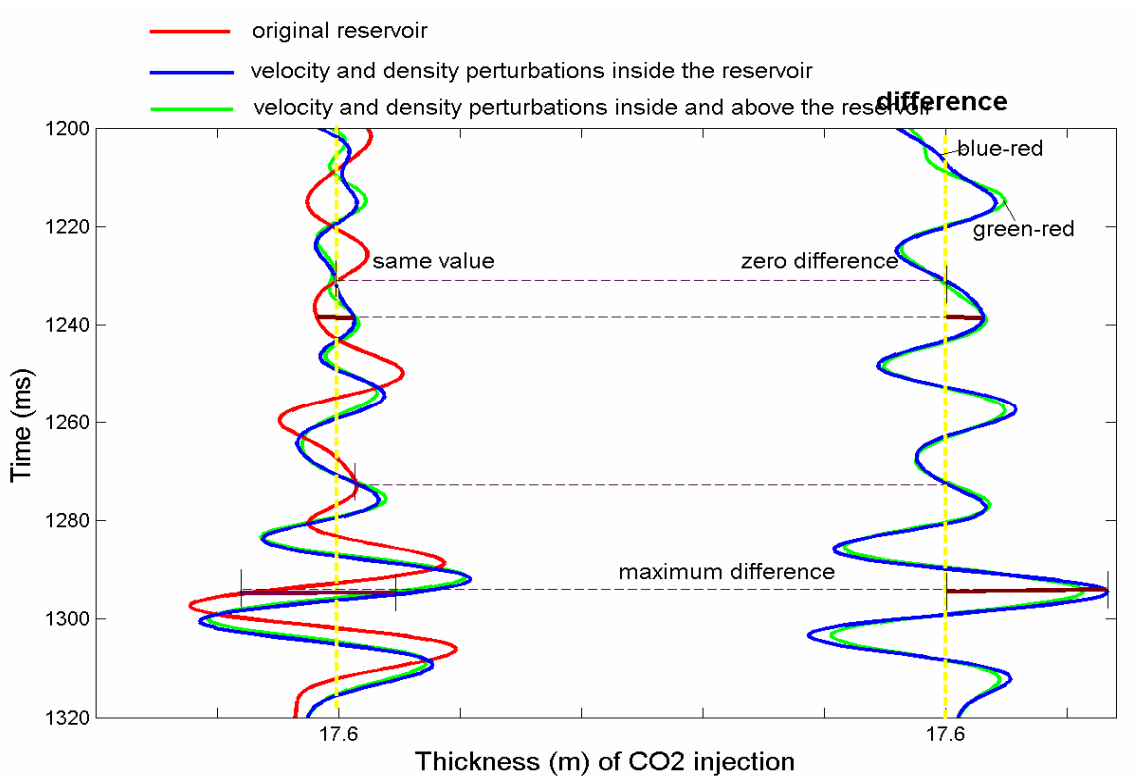

FIG. 8. Difference in trace for a 17.6 m thickness of CO_2 injection.

Time-lapse seismic differences are commonly used to map the distributions of the injected fluids. However, the difference is a simple and direct display of waveform distortion caused by medium perturbations and cannot completely represent the wave

scattering characterization. Figure 8 reproduces the seismic reflection and the corresponding difference for a 17.6 m thickness of CO_2 injection. It can be seen that the maximum difference is at about 1300 ms, which is because of the phase shift of BBR reflection (primary waves) and not the multiple scattering difference. Therefore, the large difference cannot indicate high saturation of injected CO_2 because it is due to the phase shifts of strong reflected primary waves.

The waveform distortion caused by the perturbations inside and outside the reservoir mainly takes place in the section from near the top of the reservoir to the BBR reflection. This kind of phenomenon may be related to wave localization in strong heterogeneity (Sheng, 1995), we call it time-lapse "local coda wave". The distortion of the local coda wave is highly dependent on the magnitudes of medium perturbations. A small amount of CO_2 injection or a thin injected CO_2 layer will mainly cause a time-lapse amplitude anomaly while a large amount of CO_2 injection or a thick injected CO_2 layer with large reservoir perturbations will also cause the coda wave distortion and the time sag for the BBR reflection or later events.

DISCUSSION

Production of hydrocarbons and injection of CO_2 (or other fluids) may cause rock elasticity and inelasticity deformation and result in changes in seismic velocity and attenuation. However, the relationships between velocity and attenuation and rock deformation are not well established, especially in rock collapse and compaction regions. This means that further work is needed for the porous medium deformation model. A time-lapse seismic survey is primarily interested in monitoring the changes of reservoir fluids, rather than in detecting the detailed distributions of reservoir fluids. In this study, changes of the local coda wave from near the top of the reservoir to the BBR reflection is an amplified seismic response of the reservoir and the surrounding formation perturbations because the wave has been scattered many times before leaving the reservoir (changes of localized wave or localization). Snieder and his research fellows in Colorado School of Mines have developed a technique called "coda wave interferometry" to extract the medium perturbation information from the changes in the multiple scattered waves. "Coda wave interferometry" or "local coda wave" spectroscopy is probably most suitable technique for seismic reservoir monitoring. Seismic physical analyses (scale-dependent and angle-dependent multiple scattering or anisotropic Q) for reflections from the top of the reservoir, the local coda wave, and the BBR reflection or later events, may possibly provide useful clues for the determination of distributions and levels of CO_2 injection.

ACKNOWLEDGEMENTS

The authors thank the Natural Sciences and Engineering Research Council (NSERC) and CREWES for supporting this research, and Penn West Petroleum for providing well log data at a CO_2 injection site. YL appreciates the discussions with John Zhang and Yuri Leonenko and help from staff and students in the CREWES group.

REFERENCES

Arts, R., O. Eiken, O., Chadwick, A., Zweigel, P., Van Der Meer, B., and Kirby, G., 2004, Seismic monitoring at the Sleipner underground CO_2 storage site (North sea): Geological Storage of Carbon Dioxide, Eds: S. J. Baines and R. H. Worden, 181-191, Geological Society.

Calvert, R., 2005, Insights and Methods for 4D Reservoir Monitoring and Characterization: 2005 SEG/EAGE Distinguished Instructor Short Course.

Hilterman, F. J., 2001, Seismic Amplitude Interpretation: 2001 SEG/EAGE Distinguished Instructor Short Course.

Jenkins, S. D., M. W. Waite, and M. F. Bee, 1997, Time-lapse monitoring of the Duri steamflood: A pilot and case study: The Leading Edge, **16**, 1267-1273.

Kvamme, L. B., Holt, R. M., and Nes, O. M.,1997, Acoustic velocities in unconsolidated sands: EAGE 59th conference and technical exhibition, FO30.

Li, G., 2003, Fractured reservoir modeling from seismic to simulator: A reality: The Leading Edge, **22**, 684-695.

Lines, L. R., Zou, Y., and Embleton, J., 2003, Reservoir characterization and Heavy oil production: CSEG Recorder, **26**, 26-29.

Liu, Y. and Schmitt, D. R., 2006, The Transition Between the Scale Domains of Ray and Effective Medium Theory and Anisotropy: Numerical Models: Pure and Applied Geophysics, **163**, 1327-1349.

Mavko, G., Mukerji, T., and J. Dvorkin, 1998, The rock physics handbook: Cambridge University Press.

Ng, H. T., Bentley, L. R., Krebes, E. S., 2005, Monitoring fluid injection in a carbonate pool using time-lapse analysis: Rainbow Lake case study: The Leading Edge, **22**, 530-534.

Scott Jr., T. E., Zaman, M.M., and Roegiers, J. C., 1998, Acoustic-velocity signatures associated with rock-deformation processes: JPT (June, 1998), 70-74.

Sen, V., and Settari, A., 2005, Coupled geomechanical and flow modeling of compacting reservoirs: The Leading Edge, **24**, 1284--1286.

Sheng, P., 1995, Introduction to wave scattering, localization, and mesoscopic phenomena: Academic Press, San Diego.

Tura, A., Barker, T., Cattermole, P., Collins, C., Davis, J., Hatchell, P., Koster, K., Schutjens, P., and Wills, P., 2005, Monitoring primary depletion reservoirs using amplitudes and time shifts from high-repeat seismic surveys: The Leading Edge, **24**, 1214-1221.